Fermi National Accelerator Laboratory

FERMILAB-Pub-87/144-E

Measurement of the D^0, D^+, and D_S^+ Lifetimes*

J.R. Raab[1][a], J.C. Anjos[3], J.A. Appel[5], S.B. Bracker[8], T.E. Browder[1], L.M. Cremaldi[4], J.R. Elliott[4], [b], C.O. Escobar[7], P. Estabrooks[2], M.C. Gibney[4], G.F. Hartner[8], P.E. Karchin[1],[c], B.R. Kumar[8], M.J. Losty[6], G.J. Luste[8], P.M. Mantsch[5], J.F. Martin[8], S. McHugh[1], S.R. Menary[8], R.J. Morrison[1], T. Nash[5], U. Nauenberg[4], P. Ong[8], J. Pinfold[2], G. Punkar[1], M.V. Purohit[5], A.F.S. Santoro[3], J.S. Sidhu[2],[†], K. Sliwa[5], M.D. Sokoloff[5], M.H.G. Souza[3], W.J. Spalding[5], M.E. Streetman[5], A.B. Stundžia[8], M.S. Witherell[1]

(The Tagged Photon Spectrometer Collaboration)

(1) *University of California, Santa Barbara, California 93106*
(2) *Carleton University, Ottawa, Ontario, Canada K1S5B6*
(3) *Centro Brasileiro de Pesquisas Fisicas, Rio de Janeiro, Brazil*
(4) *University of Colorado, Boulder, Colorado, USA*
(5) *Fermi National Accelerator Laboratory, Batavia, Illinois, USA*
(6) *National Research Council, Ottawa, Ontario, Canada*
(7) *Universidade de São Paulo, São Paulo, Brazil*
(8) *University of Toronto, Toronto, Ontario, Canada*

September 1987

Dedicated to the memory of our colleague

J.S. Sidhu

*Submitted to Phys.Rev.D.

MEASUREMENT OF THE D^0, D^+, AND D_s^+ LIFETIMES

J.R. Raab[1],[a], J.C. Anjos[3], J.A. Appel[5], S.B. Bracker[8], T.E. Browder[1], L.M. Cremaldi[4], J.R. Elliott[4],[b], C.O. Escobar[7], P. Estabrooks[2], M.C. Gibney[4], G.F. Hartner[8], P.E. Karchin[1],[c], B.R. Kumar[8], M.J. Losty[6], G.J. Luste[8], P.M. Mantsch[5], J.F. Martin[8], S. McHugh[1], S.R. Menary[8], R.J. Morrison[1], T. Nash[5], U. Nauenberg[4], P. Ong[8], J. Pinfold[2], G. Punkar[1], M.V. Purohit[5], A.F.S. Santoro[3], J.S. Sidhu[2],[†], K. Sliwa[5], M.D. Sokoloff[5], M.H.G. Souza[3], W.J. Spalding[5], M.E. Streetman[5], A.B. Stundžia[8], M.S. Witherell[1]

(The Tagged Photon Spectrometer Collaboration)

[1] *University of California, Santa Barbara, California, 93106*
[2] *Carleton University, Ottawa, Ontario, Canada K1S5B6*
[3] *Centro Brasileiro de Pesquisas Fisicas, Rio de Janeiro, Brazil*
[4] *University of Colorado, Boulder, Colorado, USA*
[5] *Fermi National Accelerator Laboratory, Batavia, Illinois, USA*
[6] *National Research Council, Ottawa, Ontario, Canada*
[7] *Universidade de São Paulo, São Paulo, Brazil*
[8] *University of Toronto, Toronto, Ontario, Canada*

Dedicated to the memory of our colleague

J.S. Sidhu.

ABSTRACT

We have measured the lifetimes of the D^0, D^+, and D_s^+ mesons which were produced by a high energy photon beam incident on beryllium. Using the Fermilab Tagged Photon Spectrometer with a silicon microstrip vertex detector we have collected 100 million events from which we have extracted about 4200 D^0 decays in the $K^-\pi^+$ and $K^-\pi^+\pi^-\pi^+$ modes, 3000 D^+ into the $K^-\pi^+\pi^+$ channel, and a total of 230 D_s^+ into $\phi\pi^+$ and $\overline{K}^{*0}K^+$. From an analysis of these events we have determined the lifetimes for the D^0, D^+, and D_s^+ to be $0.422 \pm 0.008 \pm 0.010$, $1.090 \pm 0.030 \pm 0.025$, and $0.47 \pm 0.04 \pm 0.02$ picoseconds, respectively.

I. INTRODUCTION

The singly charmed D^0, D^+, and D_s^+ mesons provide a unique opportunity to study the weak decays of the charm quark . Since the surprising discovery of different D^0 and D^+ lifetimes,[1] much theoretical and experimental work has been devoted to explaining and to obtaining better measurements of that difference. The lack of high statistics data on charm lifetimes has impeded the development of realistic theories and their corresponding tests. Precise measurements of the D^0, D^+, and D_s^+ lifetimes provide important constraints on the various theoretical models of charm decay.

The obstacles to precise measurements of charmed particle lifetimes have been a combination of low statistics, poor signal-to-noise ratios, and poor vertex resolution.[2] However, using the Tagged Photon Spectrometer (TPS) and silicon microstrip detectors (SMDs) we have collected a large charm-rich data sample in experiment 691 (E-691) at Fermilab. We have extracted approximately 4200 clean D^0 decays in three modes, 3000 D^+ decays in a single channel, and 230 D_s^+ events in two modes. (Throughout the paper the charge conjugate states are implicitly included.) In this article we present our final results[3] from the lifetime analysis of these events.

In section II of this paper we describe the apparatus and in section III the event reconstruction. The common elements in the event selection for the different modes is given in section IV. The method of extracting the lifetimes and the details particular to each mode are presented in section V. A discussion of systematic errors follows. In section VII we summarize our results and compare them to theoretical calculations.

II. EXPERIMENTAL APPARATUS

The TPS is a large acceptance two-magnet spectrometer which was designed and built for a previous experiment, E-516.[4] The upgraded version of the spectrometer as used by E-691 is shown in Fig. 1.

The photon beam was generated from the bremsstrahlung of 260 GeV/c electrons as they passed through a 0.2 radiation length tungsten radiator. A set of magnets behind the radiator deflected the electrons into an array of shower counters where the final electron energy was measured. From this measurement and the electron beam energy, the radiated photon energy k was deduced. The photon energy spectrum extended from 90–260 GeV, and was roughly 1/k from 100 GeV on; the mean tagged photon energy was 145 GeV.

The most significant improvement to the TPS for the E-691 run was the instal-

lation of a vertex detector assembly.[5] We used nine silicon microstrip detector planes with a 50 μm strip spacing. As shown in Fig. 2, the planes were arranged telescopically and alternately covered one of the three views, $X(0°)$, $Y(90°)$ and $V(-20.5°)$. The angular acceptance of the system was about ± 100 mrad. The signals from the strips were amplified, and discriminated at about half of the signal level produced by a minimum ionizing particle. We used modified MWPC shift register/discriminator cards to read out the strips: 3×512, 3×768, and 3×1000 channels from the upstream, middle, and downstream triplets, respectively. The downstream end of the 5 cm long beryllium target was located 2.7 cm from the first microstrip plane, and the distance between the most upstream and downstream planes was 22 cm. Because of a ~95% per plane efficiency (dead channels accounted for over half of the 5% inefficiency) and a 14 μm intrinsic transverse resolution which was much smaller than typical transverse charm decay lengths of 150 μm, we were able to resolve the secondary vertex from the primary for typically half of the charm decays.

The TPS had four drift chamber stations for downstream tracking and momentum measurements. The drift gas consisted of equal parts of argon and ethane, with a 1.5% admixture of ethanol for quenching secondary discharges. We had a total of 35 drift chamber planes covering three views, $X(0°)$, $U(20.5°)$, and $V(-20.5°)$: eight upstream of the first magnet, twelve in between the two magnets, twelve immediately downstream of the second magnet, and three in front of the calorimeters. The chamber per plane resolution and efficiency, as measured using reconstructed tracks, were about 300 μm and 90%, respectively. The upstream magnet had a horizontal and vertical acceptance of about ± 240 mrad and ± 120 mrad, and the downstream magnet of about ± 120 mrad and ± 60 mrad. The two magnets gave the charged particles horizontal momentum kicks of 0.21 and 0.32 GeV/c, respectively.

We used two threshold Čerenkov counters,[6] the upstream one with 28 cells and the downstream one with 32 cells. The upstream counter was filled with N_2 gas and had an index of refraction $n = 1.000309$. The second counter contained a mixture of 20% N_2–80% He by volume to give $n = 1.000090$. Narrow strips of baffling at beam height were stretched across the counters to absorb light from electrons created in beam photon conversions. The threshold momenta for the different particles are listed in Table I. We were able to separate pions from kaons and protons in the 6–37 GeV/c momentum region, and kaons from pions and protons between 20–37 GeV/c. The number of photo-electrons collected for highly relativistic particles was about 12

in each counter.

Two large calorimeters, a segmented lead liquid scintillator calorimeter[7] and an iron acryllic scintillator sandwich,[8] were used for electromagnetic and hadronic energy measurements. The EM calorimeter had a shower position resolution of a few millimeters and an energy resolution of about $21\%/\sqrt{E}$. We used it for π^0 and η reconstruction, and for electron identification. The hadron calorimeter had an energy resolution of about $75\%/\sqrt{E}$ and was essential to the identification of muons and neutral hadrons. Both calorimeters were used in the main trigger of the experiment—a transverse energy trigger. A linear array of shower counters placed at beam height in front of the EM calorimeter reduced the contamination of the trigger by e^+e^- pairs from beam photon conversions. Behind the hadron calorimeter a 1.0 m thick iron wall ranged out most hadrons, and was followed by a scintillator wall for muon detection.

The experiment was triggered if the total transverse energy deposited in the calorimetry was greater than about 2.2 GeV. The large transverse energy signal was required to be in coincidence with the following: a signal from a thin scintillation counter just downstream of the target to indicate the presence of at least one charged particle[9] (all signals were timed relative to the leading edge of this pulse); a light signal from the upstream Čerenkov counter to reduce false triggers from high energy muons produced in a neighbouring upstream experiment; and either a hadronic energy deposit greater then 40 GeV together with at least a 90 GeV beam photon, or—to circumvent the poor acceptance of the tagging system for very high energy photons—a hadronic energy deposit greater then 80 GeV. These requirements suppressed the false trigger rate from pair production by a factor of 200, leaving less than a 5% contamination in the final sample, and they rejected 70% of all hadronic interactions while retaining about 80% of the events with hadronic charm decays. (This was checked in detail for two-, three-, and four-body decays). The difference in transverse energy between charm events and hadronic events is best illustrated in Fig. 3. The data for Fig. 3 were obtained from the reconstruction of hadronic events taken without the transverse energy trigger.

During a three month period in 1985 we recorded about 100 million events of which 10% were taken without the transverse energy requirement. The data acquisitions were performed by a PDP-11/55 and monitored on a VAX 11/780. During a typical 22 second spill we recorded about 2000 events on magnetic tape; usual event

sizes were on the order of 1700 16-bit words. The data were reconstructed using the Fermilab Cyber system and the new microprocessor array developed by the Fermilab Advanced Computer Program.[10] The total reconstruction time per event on a single Cyber 175 was approximately 1.5 cpu seconds, and about 8 cpu seconds per microprocessor. Because 65–70% of all the data were reconstructed using this microprocessor system, the time delay to physics analysis with the full data set was reduced by a factor of three.

III. EVENT RECONSTRUCTION

Our track finding procedure started in the SMDs. This method was chosen because of the low noise, high efficiency and good resolution of the SMDs, and because the upstream field-free region had the largest number of planes; nine SMD and eight from the upstream drift chamber station in front of the first magnet.

The algorithm first searched for tracks with three hits in each SMD view. Given a set of three-hit tracks in two distinct views, the remaining view was examined at the predicted location for a three-, two-, or one-hit segment. On the next iteration three-two-one, and two-two-two type combinations were explored. For the latter, the reconstruction had to rely on the first drift chamber station for additional constraints, while needing less support for the nine-, eight-, and seven-hit segments with two 3-hit views. The track segments were then projected through the spectrometer into the drift chambers using a single bend point approximation to the magnetic fields. Before the final momentum fit was performed a search was made for 'drift chamber only' tracks from long-lived strange particles which decayed downstream of the SMDs.

For finding vertices, an accurate knowledge of the errors associated with the five track parameters (x and y intercepts, x and y slopes, and total momentum) was needed. From a detailed momentum fit we obtained

$$\frac{\Delta p}{p} \approx \quad 0.05\% p + 0.5\%,$$

and from a fit to only SMD hits we found for typical errors at the downstream end of the target ($z \simeq 0$)

$$\sigma_x(z=0) \simeq 13 + \frac{50}{p(GeV/c)}\ \mu m \qquad \sigma_{s_x}(z=0) \simeq 0.10 + \frac{3.3}{p(GeV/c)}\ mrad$$

$$\sigma_y(z=0) \simeq 16 + \frac{50}{p(GeV/c)}\ \mu m \qquad \sigma_{s_y}(z=0) \simeq 0.13 + \frac{3.3}{p(GeV/c)}\ mrad$$

For the slope and intercept, the second term in the errors accounted for multiple scattering in the target and was essentially negligible for tracks with momenta greater than 5 GeV/c. The last term in the momentum error stemmed from multiple scattering in the downstream spectrometer. For tracks which did not pass through the second magnet the momentum resolution was worse by a factor of two, $\frac{\Delta p}{p} \approx 0.1\% p$.

The vertexing algorithm took any two tracks with SMD hits and fit them to a common vertex using a least-squares method. As long as the chi-square per degree-of-freedom of the fit remained below 3.0 other tracks were added—one by one—to the fit. If the additional track pulled the chi-square over the threshold it was excluded from the current vertex but could still be included in another. A charm event as reconstructed in the SMDs is shown in Fig. 4. Typical errors on the vertices were approximately 15 μm transverse to the beam and 300 μm along the beam.

The charged hadrons were identified in the two Čerenkov counters. At the start of the Čerenkov reconstruction all tracks were assigned an *a priori* probability of 0.02, 0.01, 0.81, 0.12, 0.04 to be an electron, muon, pion, kaon, or proton, respectively. These *a priori* probabilities corresponded to the average fractional occurrence of these particles in a typical hadronic interaction. A fit to the observed light distributions and light levels in the counters either raised or lowered these probability assignments, depending on whether the detected radiation was compatible or incompatible with a given mass hypothesis.

The reconstruction of showers in the electromagnetic calorimeter used a regression algorithm described in detail elsewhere.[11] Hadronic and electromagnetic particles were identified in the calorimetry by their characteristic shower shapes and penetration depths. The reconstruction efficiency for electrons with energy greater than 12 GeV was about 70%, and the detection and reconstruction efficiency for neutral pions with energy greater than 12 GeV was about 25% for clean low multiplicity events, but only 10–11% for charm events.

IV. EVENT SELECTION

In the first step of the selection we imposed general criteria on track quality, particle identification, and invariant mass. In the second step we applied vertex cuts which dramatically reduced the background, and we limited our fiducial volume to avoid regions of different efficiency.

We required that the number of degrees-of-freedom in the track fit be at least 12 out of a maximum of 39, or that the chi-square of the fit be less than 8.0, or both. These cuts eliminated most spurious tracks for which a small number of hits had accidentally lined up. In order to make a vertex we demanded that the tracks were detected in the SMDs. Almost all tracks were required to pass through the upstream Čerenkov counter, so that some information on the particle identity was available; for two-particle mass combinations we required that the tracks pass through the second Čerenkov counter, while for three or more particle combinations we allowed for the escape of a single track into the region between the central two drift chamber stations. For each decay mode, there was a minimum requirement on the product of the Čerenkov probabilities. The cuts on the joint probability were chosen to optimize the statistical significance of the signal. None of the lifetime results were sensitive to small changes in these cuts. The criterion always forced at least one particle to have a Čerenkov probability above the *a priori* assignment, and for the two-kaon D_s^+ modes constrained both kaons to be above their *a priori* probabilities. In Fig. 5 we show the joint probability distribution for $D^0 \to K^-\pi^+$ candidates. The cut, marked by the arrow, is well separated from the *a priori* peaks.

We demanded that the tracks of the charm candidate form a good vertex, with a chi-square per degree-of-freedom less than 3.0. The remaining tracks in the event were combined into possible primary vertices. A search was made for all primary vertex candidates within a transverse distance of 75 μm from the line of flight of the reconstructed charm candidate. This selection on maximum transverse miss distance, or pointback, reduced the background by more than 60% while retaining about 80% of the charm decays. To further reduce the non-charm background, we kept only charm candidates that decayed at least a longitudinal distance z_{min} downstream of the primary vertex. The distance z_{min} was chosen to be 5–10 σ_z, depending on the decay mode, where σ_z is the longitudinal error on the distance L between the primary and the potential charm vertex as shown in Fig. 6. The value of σ_z was typically 300 μm for a D momentum of 60 GeV/c, corresponding to a proper time resolution of about 0.03 ps. The longitudinal errors on the vertices increased almost linearly with momentum due to the time dilation factor γ, but the significance of the vertex separations L/σ_z and the proper time resolution were essentially constant.

In Fig. 7 we show a scatter plot of $\Delta z/\sigma_z$ versus mass for the $K\pi$ mass combinations, where Δz was the separation of the vertices in z. The enhancement at the D^0 mass is evident. The effect of increasing z_{min} on the signal and background is

illustrated in Fig. 8. In the 20% of the events with multiple primary vertex candidates, z_{min} was computed from the most downstream one to ensure that the chosen primary was not upstream of the true production point.

We calculated the proper time t from the point which was the distance z_{min} downstream of the primary vertex to the observed decay vertex,

$$t = \frac{1}{\gamma v}(L - L_{min}),$$

where L_{min} is the distance in the flight direction corresponding to z_{min}. The shape of the time distribution was therefore insensitive to inaccuracies in the primary vertex position which were less than z_{min}. (From our Monte Carlo simulation we found that mistakes larger than z_{min} occurred in about 1% of the events.) The fiducial region for decays was defined to end at the first SMD plane to avoid the region of partial detection and reconstruction efficiency beyond. In the D^0 and D_s^+ analysis we used only events for which the proper time corresponding to the end of this region, t_{max}, was larger than the maximum time used in the fit, 2.0 ps. For the D^+, the fit to the time spectrum extended to a maximum decay time of 4.0 ps, or about four lifetimes. As for the D^0 and D_s^+ we rejected events with $t_{max} < 2.0$ ps, but because of the longer D^+ lifetime and the extended time interval of the fit there was some loss of events at long lifetimes due to decays beyond the end of the fiducial region. This effect corresponded to a reduced, albeit calculable, efficiency between 2.0 and 4.0 ps, and was taken into account in the maximum likelihood fit to the spectrum as described below.

V. LIFETIME ANALYSIS

We made a maximum likelihood fit to the proper time distributions of the form

$$N \times \frac{f(t)e^{-t/\tau}}{\int_0^{t_0} dt\ f(t)e^{-t/\tau}} + B(t),$$

where t_0 was the maximum time in the histogram, and where $B(t)$ was obtained from the time distribution of the background, as determined from events above and below the D-mass region in the mass plot, and was normalized to the signal region. The function $f(t)$, which was obtained from the Monte Carlo, corrected for effects of absorption of the decay products, acceptance, resolution, and efficiency. We found that a linear function in t was a good parameterization for this correction,[12]

$$f(t) = \begin{cases} 1. + a(t - 1.5) & t \leq 1.5 \text{ ps} \\ 1. & t > 1.5 \text{ ps.} \end{cases}$$

This form was suggested by a calculation of the effects of absorption and acceptance of the decay products. Neglecting all other inefficiencies, absorption caused an exponential turn-on which became asymptotically flat near 1.5 ps. The slope a varied from mode to mode, and was determined from the Monte Carlo simulation. The free parameters in the fit were N—the number of events in the charm signal, and τ—the charm lifetime. The likelihood function was

$$\mathcal{L} = \prod_{i=1}^{k} \frac{(N_i)^{n_i}}{n_i!} e^{-N_i}$$

where N_i and n_i were, respectively, the predicted and observed number of events in bin i, corresponding to time t_i, and k was the number of bins, 20 in every case. For all modes we obtained good fits with a χ^2 per degree of freedom near one.

A. D^0 Analysis

For the D^0 lifetime study we used three modes:

$$D^{*+} \to \pi^+ D^0,\ D^0 \to K^-\pi^+ \qquad (A)$$

$$D^{*+} \to \pi^+ D^0,\ D^0 \to K^-\pi^+\pi^-\pi^+ \qquad (B)$$

$$D^0 \to K^-\pi^+,\ (\text{no } D^{*+}) \qquad (C)$$

Events which satisfied the requirements for set (A) were excluded from set (C), so the samples were statistically independent. For set (A) the mass difference $m(D^{*+}) - m(D^0)$ was required to be between 0.144 and 0.147 GeV/c^2, and between 0.1435 and 0.1475 GeV/c^2 for set (B). Table II presents the number of signal and background events in the mass range 1.842–1.886 GeV/c^2, the minimum decay length z_{min} used for each mode, and the lifetime results obtained from the maximum likelihood fit. The mass distributions for the events which satisfied the vertex cuts are shown in Fig. 9. The slope a was 0.05, 0.20, 0.08 (ps)$^{-1}$ for samples (A), (B), and (C), respectively.

The proper time distributions for the three D^0 channels after background subtraction are illustrated in Fig. 10. They have the expected exponential form. Considering that the channels had different corrections and backgrounds, the agreement of these three measurements within statistical errors provided confirmation as to the consistency of our method. A combined fit to all three samples gave the value, $\tau(D^0) = 0.422 \pm 0.008$ ps, for the D^0 lifetime.

B. D^+ Analysis

The decay mode

$$D^+ \to K^-\pi^+\pi^+ \qquad (D)$$

was used for the D^+ lifetime study. The mass spectrum for the accepted events, using a minimum decay length $z_{min} = 10\sigma_z$, is shown in Fig. 11. Due to the cut on the vertex separation z_{min}, we obtained a background reduction factor of about 300. There were 2992±55 D^+ events in the selected mass region between 1.846 and 1.890 GeV. The number of background events, as determined from the number of events outside the D^+ region, was 1354 ± 20.

The function $f(t)$ had two parts: the first, identical in form to that given above, accounted for losses at short times with slope $a = 0.17$ $(\text{ps})^{-1}$; the second corrected for the loss of long-lived events. The latter was derived from the data and agreed with that obtained from the Monte Carlo. Because of the limited fiducial volume, the detection efficiency $\epsilon(t)$ was less than one for decays with $t \geq 2.0$ ps, and was given by the ratio of events which survived the fiducial cut at time t divided by the total. The resulting efficiency dropped linearly and was determined to be $\epsilon(t)$=1.0−0.22 t, for $t \geq 2.0$ ps, and $\epsilon(t)$=1.0 for $t < 2.0$ ps. The D^+ time distribution is shown in Fig. 12. The maximum likelihood fit gave a lifetime of 1.09 ± 0.03 ps.

C. D_s^+ Analysis

For the D_s^+ lifetime analysis, we used events consistent with one of the two decay modes,

$$D_s^+ \to \phi\pi^+ \qquad (E)$$

$$D_s^+ \to \overline{K}^{*0}K^+. \qquad (F)$$

For channel (E) we required the K^-K^+ mass to be in the interval $1.012-1.027$ GeV/c^2. The angular distribution for the decay $\phi \to K^-K^+$ is $dN/d(\cos\theta) = A\cos^2\theta$ where θ is the angle between the K^- and π^+ in the ϕ rest frame. We required $|\cos\theta| > 0.3$, which retained 97% of the signal and 70% of the background. For channel (F) we required the $K^-\pi^+$ mass to be in the interval $0.845-0.945$GeV/c^2. This range missed some of the K^* events but minimized the background. Again, we demanded that $|\cos\theta| > 0.3$, where θ is the decay angle between the K^- and K^+ in the K^* rest frame. There were no events in common mainly because of the vector meson mass constraints, and because we did not use the few ambiguous events. In both samples we discarded

events which were consistent with reflections due to K–π misidentification in the decays $D^{*+}(D^+) \to K^-\pi^+\pi^+$.

The mass distributions for both modes are shown in Fig. 13. In each plot there are clear peaks for the D_s^+ decay and for the Cabibbo-suppressed D^+ decay.[13] The time distributions for events in the mass region $1.953 - 1.985$ GeV/c^2 are shown in Fig. 14. In Table III we list the minimum longitudinal vertex separation significance, the number of signal and background events between 1.953 and 1.985 GeV/c^2, and the lifetimes as obtained from the fit. A joint fit to both distributions gave 0.47 ± 0.04 ps for the lifetime. For these modes the function $f(t)$ had a slope $a = 0.27$ (ps)$^{-1}$ and $a = 0.23$ (ps)$^{-1}$, respectively.

VI. SYSTEMATIC ERRORS

We made a thorough analysis of our systematic errors using the data sample itself and the Monte Carlo (MC) simulation. The major sources of systematic errors were the background subtraction and the correction function $f(t)$. The shifts in lifetime due to the background subtraction and the correction function were in opposite directions and tended to cancel; in any case, the effect of $f(t)$ was always less than 15% of the lifetime.

A. Background Subtraction

In the fit we floated the sum of the signal and background events. Thus, the statistical fluctuations in the background were included in the statistical error of the fit. However, there is an error associated with the average number of background events obtained from the finite number of events outside the signal region. Therefore, we had to include the errors on this average as systematic errors. For the D^* mode (A) the background subtraction had a negligible effect because of the small background and the very small lifetime difference between signal and background; it shifted the lifetime by $+0.013 \pm 0.001$ ps. For channels (B) and (C), it produced a shift of $+0.041 \pm 0.004$ and $+0.035 \pm 0.002$ ps, respectively. The errors were estimated by changing the number of background events by two standard deviations in either direction. Thus, the total effect of the background subtraction on the average D^0 lifetime was a shift of $+0.030 \pm 0.002$ ps. The background subtraction played a much larger role for the D^+ because the background had a considerably shorter effective lifetime than the signal. The total change amounted to $+0.275 \pm 0.017$ ps. For the D_s^+ the shifts for modes (E) and (F)

were $+0.08 \pm 0.02$ and 0.03 ± 0.01 ps, respectively, and produced an integrated shift of $+0.060 \pm 0.015$ ps.

B. Correction Function

The correction function accounted for the loss of events at short times due to absorption, acceptance, resolution and vertex cuts. The size of the correction was obtained from the MC, and compared to direct estimates. The reconstructed MC samples had at least four times as many events as the data.

The MC generated charm according to the photon-gluon fusion model.[14] The LUND[15] model was used to hadronize the quarks and gluons. The TPS was simulated in great detail—from multiple scattering in the target and SMDs down to the last dead drift chamber channel. The MC events were digitized, and then reconstructed with the same programs as those used for the data. In Fig. 15 we show a comparison between the data and the MC for the $D^{*+} \to D^0\pi^+, D^0 \to K^-\pi^+$ mode. At this level there is good agreement. In Fig. 16 we have plotted the difference between the reconstructed proper time and the generated MC time. The width of this distribution is a direct measure of the proper time resolution. We tested our sensitivity to the production model by fitting the lifetimes in different momentum regions. The results are presented in Table IV (a). Table IV (b) gives the measured lifetimes for different bins in the number of reconstructed vertices. Changes in the charged particle multiplicity had no effect on the observed lifetimes. We do not observe any significant systematic trends outside the statistical errors.

In Table V we list the contributions to the slope a from various sources. The last two columns contain the total a, as obtained from the MC, and the corresponding shifts in lifetime. The effect of absorption of decay particles in the target, denoted by a_{abs}, was computed from known cross sections,[16] and typically accounted for one half to one third of the total correction. The detection of long-lived, as compared with short-lived, decays was enhanced by absorption because the decay products had less material to traverse, and thus were less likely to interact. We neglected the absorption of the charmed particles because of the smaller cross sections. We also estimated the effect of the differing geometric acceptance between the upstream and downstream ends of the target by moving the decay upstream until, either, one of the wide angle decay products did not pass through the SMDs, or, the end of the target was reached. This effect also biased against upstream decays and short lived ones. The acceptance contribution to the correction, a_{acc}, was fairly small, and increased slightly with the

particle multiplicity of the decay.

In Table V we include the effect of the z_{min} vertex cuts on the corrected lifetimes; this was a higher order effect because of the small momentum dependence of the vertex errors from multiple scattering. We were completely insensitive to the cuts on the chi-square of the charm vertex and on the pointback. The estimated contribution to the correction a_z due to the z_{min} cut is listed in column four of Table V. We also investigated the shifts in lifetime due to selecting the wrong primary vertex. From the MC we found that in D^* events less than $1\frac{1}{2}\%$ of the events had the real primary vertex outside z_{min}; in the other modes this occurred for less than $\frac{1}{2}\%$ of the events. The column, titled a_{fvtx}, in Table V gives an estimate of the size of this effect. Upon adding columns two through five and the errors in quadrature to obtain column six in Table V we note that this semi-quantitative approach is in fair agreement with the corrections obtained directly from the MC. The MC results were the most reliable measurement of the correction for all effects, and were used in the lifetime fits.

As a consistency check the correction for the inefficiency at long decay times of the D^+ was crudely estimated from geometric considerations alone. From the agreement between the data, the MC, and the naive calculation we estimated our error on the slope of the efficiency function at 10%, corresponding to a negligible error on the D^+ lifetime of ± 0.003 ps.

The input lifetimes to the MC were 0.44, 1.10, 0.40 ps for the D^0, D^+, and D_s^+, respectively. From studies on the D_s^+ and the D^+ we found that the final lifetime results were not very sensitive to changes in the input MC lifetime. A 20% change of the MC D_s^+ lifetime from 0.40 ps to 0.48 ps did not change the final D_s^+ result, and a 15% shift in the D^+ MC lifetime changed the corrected D^+ lifetime well within statistical errors.

C. Misidentification

Because we had almost full particle identification capabilities in the appropriate momentum region, and because we used only well-identified particles, we did not have the visible reflections which are common in e^+e^- experiments. In fixed target experiments the reflections are also much broader due to the larger range in lab momenta of the particles. The $KK\pi$ decay modes of the D_s^+ are most sensitive to π-K misidentification which causes the reflection of the $D^+ \to K^-\pi^+\pi^+$ decays to produce a longer effective D_s^+ lifetime, and to p-K confusion which reflects the Λ_c^+ down and shifts the

observed lifetime down. These reflections had a width of a few hundred MeV/c^2, much wider than the widths of the mass peaks. On account of these difficulties we used only the resonant modes, (E) and (F), rather than including the nonresonant events for the D_s^+ lifetime measurement. Extensive studies using both data and MC showed that about two events and one event, in both modes combined, could be attributed to the above sources, respectively. In addition, the background subtraction reduced this effect further, so that the feedthrough contributions to the total systematic error were negligible.

Combining all the above errors in quadrature, we estimate our total systematic errors on the lifetime measurements of the D^0, D^+, D_s^+ at 0.010, 0.025, and 0.02 ps, respectively.

VII. SUMMARY AND CONCLUSIONS

Our lifetimes for the D^0, D^+, and D_s^+ are summarized in Table VI. The D^0 and D^+ measurements are consistent with our previous results,[3] and the world averages[17] of $0.43^{+0.05}_{-0.04}$ ps and $0.94^{+0.11}_{-0.08}$ ps, respectively. The D_s^+ lifetime is almost twice the world average of $0.28^{+0.16}_{-0.07}$ ps, although it is in better agreement with more recent measurements.[18] We observe that the D^0 and the D_s^+ lifetimes are equal within errors, which may indicate a fundamental similarity in the decay processes.

For comparison with theoretical models and partial decay widths, we have computed our lifetime ratios $\tau(D_s^+)/\tau(D^0) = 1.11 \pm 0.10 \pm 0.04$ and $\tau(D^+)/\tau(D^0) = 2.58 \pm 0.09 \pm 0.08$. This latter ratio has been inferred from semi-leptonic branching ratios;[1] ignoring the Cabibbo-suppressed annihilation process with final state leptons for the D^+,

$$\begin{aligned}\tau(D^+)/\tau(D^0) =& Br(D^+ \to e^+X)/Br(D^0 \to e^+X)\\ =& 2.3^{+0.5}_{-0.4} \pm 0.1,\end{aligned}$$

as measured by Mark III.[19]

The spectator quark model[20] correctly predicts the order of magnitude of charm particle lifetimes, but in its simplicity fails to account for the different observed lifetimes. To explain these differences various attempts have been made to improve the model either by suppressing the D^+ decays, or enhancing the D^0 modes, or both.

The suppression of the D^+ decays is achieved via destructive interference of two amplitudes with identical final states.[21] The enhancement of the D^0 is accomplished by

increasing the contribution of the W exchange process. This process is usually ignored because of the helicity suppression at the light quark vertex and because of the required large overlap of the quark wave functions in the original hadron. However, some models claim that gluon radiation removes those constraints.[22] In another approach[23] it has been proposed that there is a sizable general non-leptonic enhancement of all charm decays from QCD corrections which is almost exactly cancelled by the interference effect for the D^+. It is uncertain what influence final state interactions have on the lifetimes;[24] that they play an important role for individual decay modes seems to be substantiated by the large $D^0 \to \phi\overline{K}^0$ branching ratio.[25]

The various models make different predictions for the D_s^+ semi-leptonic branching ratios and lifetime. If W exchange/annihilation is dominant, then a large semi-leptonic branching ratio for $D_s^+ \to Xe^+\nu$ is expected, and the D_s^+ lifetime should be less than or equal to that of the D^0.[26] The interference effect alone, while partially explaining the D^0–D^+ lifetime discrepancy, cannot reproduce the small semi-leptonic branching ratio of the D^0 as observed by Mark III.[19] However, interference together with non-leptonic enhancement from QCD corrections could account for the observed semi-leptonic branching ratios and lifetimes.

Lifetime measurements alone are insufficient to distinguish clearly among the different models. For example, the W annihilation/exchange mechanism predicts lifetime ratios, but contains two free parameters which determine the strength of the colour singlet and octet couplings to the emitted gluon. Now that detailed predictions of branching ratios are available,[23,27,28] it is expected that precise measurements of semi- and non-leptonic modes, especially those of the D_s^+, together with the lifetimes, will lead to a concise picture of charm decay.

This research was supported by the U.S. Department of Energy, by the Natural Science and Engineering Research Council of Canada through the Institute of Particle Physics, by the National Research Council of Canada, and by the Brazilian Conselho Nacional do Desenvolvimento Cientifico e Tecnologico.

REFERENCES

(a) Now at CERN, Division EP, CH-1211 Genève, Switzerland.
(b) Present address: Electromagnetic Applications, Inc., Denver, CO.
(c) New address: Yale University, New Haven, Connecticut.
(†) Deceased.

[1] For early lifetime ratio measurements see W. Bacino *et al.*, Phys. Rev. Let., **45**, 329 (1980); D. Allasia *et al.*, Nucl. Phys., **B176**, 13 (1980).
[2] For reviews refer to V. Lüth, SLAC Report SLAC-PUB-4052, 1986 (unpublished); C. Caso and M. C. Touboul, Rev. Nuovo Cimento **12**, (1986).
[3] See our previously published results, J. C. Anjos *et al.*, Phys. Rev. Lett., **58**, 311 (1987); **58**, 1818 (1987).
[4] K. Sliwa *et al.*, Phys. Rev. D **32**, 1053 (1985), and references therein.
[5] P. Karchin *et al.*, IEEE Trans. Nucl. Sci. **32**, 612 (1985).
[6] D. Bartlett *et al.*, University of Colorado Report COLO-HEP-121, 1986 (to be published in Nucl. Instrum. & Methods).
[7] V. Bharadwaj *et al.*, Nucl. Instrum. & Methods **228**, 283 (1985).
[8] J. Appel, P. Mantsch, M. Streetman, R. Robertson, Nucl. Instrum. & Methods **A243**, 361 (1986).
[9] The threshold was set at 1.5 minimum ionizing to allow for dimuon studies; see M. D. Sokoloff *et al.*, Phys. Rev. Lett. **57**, 3003 (1986).
[10] I. Gaines and T. Nash, Fermilab Report FERMILAB-Pub-87/38, 1987 (submitted to Annu. Rev. Nucl. & Part. Sci.).
[11] D. Summers, Nucl. Instrum. & Methods **228**, 290 (1985).
[12] For details see J. Raab, Ph.D. Thesis, University of California at Santa Barbara Report UCSB-HEP-87-8, 1987 (unpublished).
[13] These events have been used to measure the relative branching fractions for these modes; M. Witherell, in *Heavy Quark Physics*, proceedings of the 1987 Meeting of the American Physical Society, Division of Particles and Fields, Salt Lake City, Utah.
[14] M. Fontannaz, B. Pire, and D. Schiff, Z. Phys. C **11**, 201 (1981); L. M. Jones and H. W. Wyld, Phys. Rev. D **17**, 759 (1978); P. Aurenche *et al.*, Nucl. Phys. **B286**, 553 (1987).
[15] T. Sjöstrand, University of Lund Report LU-TP-85-10, 1985, (unpublished); also see, B. Andersson, G. Gustafson, C. Ingelman, and T. Sjöstrand, Phys. Rep. **97**, 1 (1983).
[16] We used the absorption cross sections as given by S. Denisov *et al.*, Nucl. Phys. **B61**, 62 (1973).
[17] M. Aguilar-Benitez *et al.*, (Particle Data Group), Phys. Lett. **170B**, 1 (1986), and references therein.
[18] C. Jung *et al.*, Phys. Rev. Lett. **56**, 1775 (1986); N. Ushida *et al.*, Phys. Rev. Lett. **56**, 1767 (1986); S. E. Csorna *et al.*, Contribution to the XXIII Int'l Conference in High Energy Physics, Berkeley, California, 1986; D. P. Kelsey, Contribution to the XXI EPS Conference, Uppsala, Sweden, 1987.
[19] R. M. Baltrusaitis *et al.*, Phys. Rev. Lett. **54**, 1976 (1985).
[20] As described in M. K. Gaillard, B. W. Lee, and J. L. Rosner, Rev. Mod. Phys. **47**,

277 (1975).
[21] N. Bilić, B. Guberina, and J. Trampetić, Nucl. Phys. **B248**, 261 (1984); B. Guberina, S. Nussinov, R. Peccei, and R. Rũckl, Phys. Lett. **89B**, 111 (1979).
[22] M. Bander, D. Silverman, and A. Soni, Phys. Rev. Lett. **44**, 7 (1980); H. Fritzsch and P. Minkowski, Phys. Lett. **90B**; 455 (1980); K. Shizuya, Phys. Lett. **100B**, 79 (1981).
[23] M. A. Shifman and M. B. Voloshin, Institute of Theoretical and Experimental Physics Report No. ITEP-86-83, Moscow, 1983 (unpublished); M. B. Voloshin and M. A. Shifman, Sov. J. Nucl. Phys. **41**, 120 (1985); **64**, 698 (1986).
[24] C. Sorenson, Phys. Rev. D **23**, 2618 (1981).
[25] J. F. Donoghue, Phys. Rev. D **33**, 1516 (1986).
[26] R. Rũckl, Habilitationsschrift, Universität Mũnchen, 1983 (unpublished).
[27] A. Buras, Nucl. Phys. **B268**, 16 (1986).
[28] M. Bauer, B. Stech, and M. Wirbel, Z. Phys. C **34**, 103 (1986).

FIGURE CAPTIONS

Fig. 1. Plan view of the Tagged Photon Spectrometer at Fermilab.

Fig. 2. Arrangement of the microstrip planes.

Fig. 3. Transverse energy of (a) all hadronic events (b) reconstructed charm events as obtained from data without the transverse energy trigger.

Fig. 4. A charm event as reconstructed in the SMDs. A $\overline{D}^0 \to K^+\pi^-$, the additional π^- is from $D^{*-} \to \overline{D}^0\pi^-$; the ellipses represent the one sigma errors on the vertex position.

Fig. 5. Joint Čerenkov probability distribution for $D^0 \to K^-\pi^+$ candidates. The arrow marks the cut used in the event selection.

Fig. 6. Schematic of a production (primary) and a decay (secondary) vertex, and definitions of associated variables.

Fig. 7. Scatter plot of $\Delta z/\sigma_z$ vs $K^+\pi^-$ invariant mass. Note the higher density in the band centered at the D^0 mass.

Fig. 8. The $K^+\pi^-$ invariant mass at four different values of $\Delta z/\sigma_z$.

Fig. 9. Invariant mass spectra for the three D^0 channels with vertex cuts as described in the text: (a) $D^{*+} \to \pi^+D^0$, $D^0 \to K^-\pi^+$; (b) $D^{*+} \to \pi^+D^0$, $D^0 \to K^-\pi^+\pi^-\pi^+$; and (c) $D^0 \to K^-\pi^+$, no D^{*+}.

Fig. 10. Proper time spectra for the three D^0 channels, in the same order as in Fig. 9. The data points are shown with background subtracted. The error bars represent the statistical error, including that on the background. The smooth curve represents the best fit as described in the text.

Fig. 11. Invariant mass spectrum for $K^-\pi^+\pi^+$ for events used in the D^+ lifetime measurement.

Fig. 12. Proper time spectrum for D^+ events. The data points are shown with background subtracted as in Fig. 10. The smooth curve represents the best fit as described in the text.

Fig. 13. Invariant mass spectra for two D_s^+ channels with vertex cuts as described in the text: (a) $D_s^+ \to \phi\pi^+$, $\phi \to K^+K^-$ and (b) $D_s^+ \to \overline{K}^{*0}K^+$, $\overline{K}^{*0} \to K^-\pi^+$.

Fig. 14. Proper time spectra for the two D_s^+ samples, arranged in the same order as in Fig. 13. The data points are shown with background subtracted. The error bars represent the statistical error, including that on the background. The smooth curve follows the best fit as described in the text.

Fig. 15. Comparison of Monte Carlo (- - -) and background subtracted data (—) for the $D^{*+} \rightarrow \pi^+ D^0$, $D^0 \rightarrow K^- \pi^+$ modes: (a) number of tracks per event (b) number of vertices per event (c) total momentum (d) chi-square of the secondary vertex (e) pointback.

Fig. 16. Difference between the generated Monte Carlo proper time and the reconstructed proper time.

TABLE CAPTIONS

Table I Threshold momenta for particles in the upstream and downstream Čerenkov counters.

Table II Characteristics of the D^0 samples; the errors are statistical.

Table III Characteristics of the D_s^+ samples; the errors are statistical.

Table IV a The lifetimes (ps) for different momentum intervals.

Table IV b The lifetimes (ps) for different vertex multiplicity intervals.

Table V Contributions to the parameter a (ps^{-1}) in the correction function $f(t)$: direct estimates and the Monte Carlo results. The quantity $\Delta\tau_{MC}$ is the shift in lifetime in ps.

Table VI Summary of the D lifetimes.

TABLE I Threshold momenta for particles in the upstream and downstream Čerenkov counters.

counter	threshold momenta (GeV/c) for e	μ	π	K	p
upstream	0.02	4.2	5.6	20.0	37.7
downstream	0.04	7.9	10.4	37.0	69.8

TABLE II Characteristics of the D^0 samples; the errors are statistical.

Mode	z_{min}/σ_z	No. Signal	No. Background	Lifetime (ps)
(A)	5	1210 ± 36	94 ± 5	0.417 ± 0.014
(B)	7	700 ± 27	113 ± 5	0.437 ± 0.019
(C)	8	2302 ± 48	768 ± 14	0.420 ± 0.011

TABLE III Characteristics of the D_s^+ samples; the errors are statistical.

Mode	z_{min}/σ_z	No. Signal	No. Background	Lifetime (ps)
(E)	7.5	143 ± 14	49 ± 4	$0.45^{+0.05}_{-0.04}$
(F)	10	85 ± 11	26 ± 3	$0.49^{+0.08}_{-0.06}$

TABLE IV (a) The lifetimes (ps) for different momentum intervals

Particle	momentum regions 20–58 GeV/c	58–68 GeV/c	68–140 GeV/c
D^0	0.42 ± 0.02	0.41 ± 0.03	0.42 ± 0.02
D^+	1.06 ± 0.06	1.09 ± 0.05	1.06 ± 0.04
D_s^+	0.53 ± 0.10	0.38 ± 0.07	0.46 ± 0.08

TABLE IV (b) The lifetimes (ps) for different vertex multiplicity intervals

Particle	number of reconstructed vertices 2	3–4	5–18
D^0	0.42 ± 0.02	0.42 ± 0.03	0.44 ± 0.03
D^+	1.04 ± 0.03	1.17 ± 0.07	1.06 ± 0.09
D_s^+	0.52 ± 0.09	0.45 ± 0.07	0.43 ± 0.12

TABLE V Contributions to the parameter a (ps^{-1}) in the correction function $f(t)$: direct estimates and the Monte Carlo results. The quantity $\Delta\tau_{MC}$ is the shift in lifetime in ps.

mode	a_{abs}	a_{acc}	a_z	a_{fvtx}	a_{tot}	a_{MC}	$\Delta\tau_{MC}$
(A)	.04 ±.01	.015 ±.010	.01 ±.02	.02 ±.01	.08 ±.03	.05 ±.02	.010 ±.004
(B)	.10 ±.015	.04 ±.02	.05 ±.030	.03 ±.02	.22 ±.04	.20 ±.03	.050 ±.008
(C)	.04 ±.01	.015 ±.010	.05 ±.02	.01 ±.01	.11 ±.03	.08 ±.02	.014 ±.004
(D)	.07 ±.01	.02 ±.01	.04 ±.02	.00 ±.01	.13 ±.03	.17 ±.02	.14 ±.02
(E)	.08 ±.01	.03 ±.02	.04 ±.05	.02 ±.01	.17 ±.06	.27 ±.05	.080 ±.017
(F)	.08 ±.01	.03 ±.02	.04 ±.05	.02 ±.01	.17 ±.06	.23 ±.05	.080 ±.017

TABLE VI Summary of the D lifetimes

Particle	Lifetime (ps)	stat. error (ps)	sys. error (ps)
D^0	0.422	± 0.008	± 0.010
D^+	1.090	± 0.030	± 0.025
D_s^+	0.47	± 0.04	± 0.02

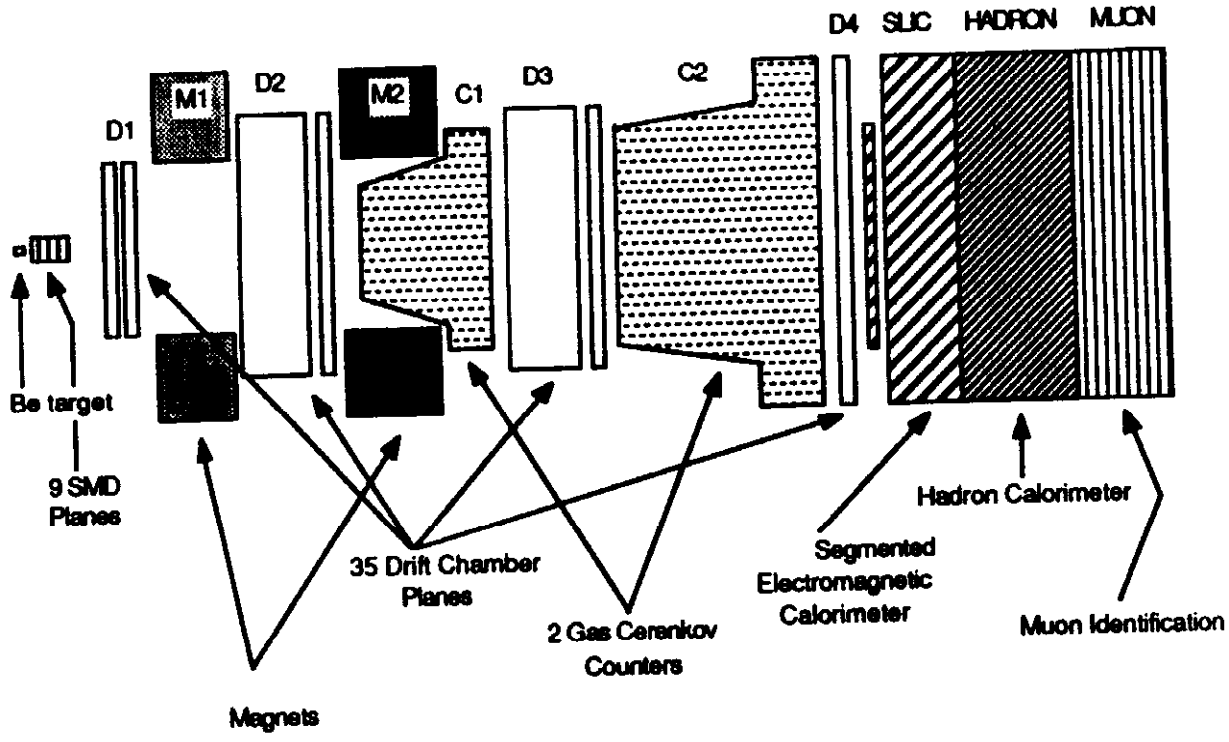
D4
SLIC
HADRON
MUON
M1
D2
M2
C1
D3
C2
D1
Be target
9 SMD Planes
35 Drift Chamber Planes
Magnets
2 Gas Cerenkov Counters
Segmented Electromagnetic Calorimeter
Hadron Calorimeter
Muon Identification

Figure 1.

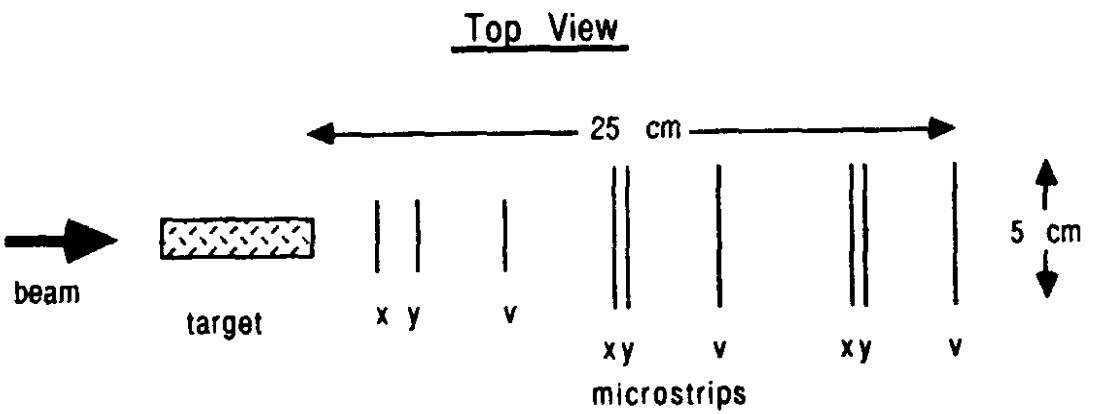

Figure 2.

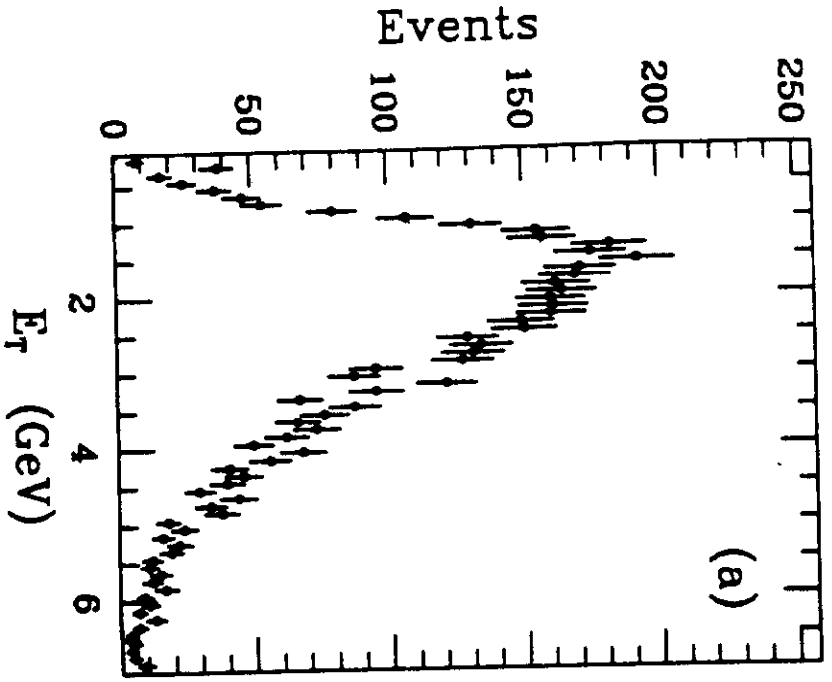

Figure 3a

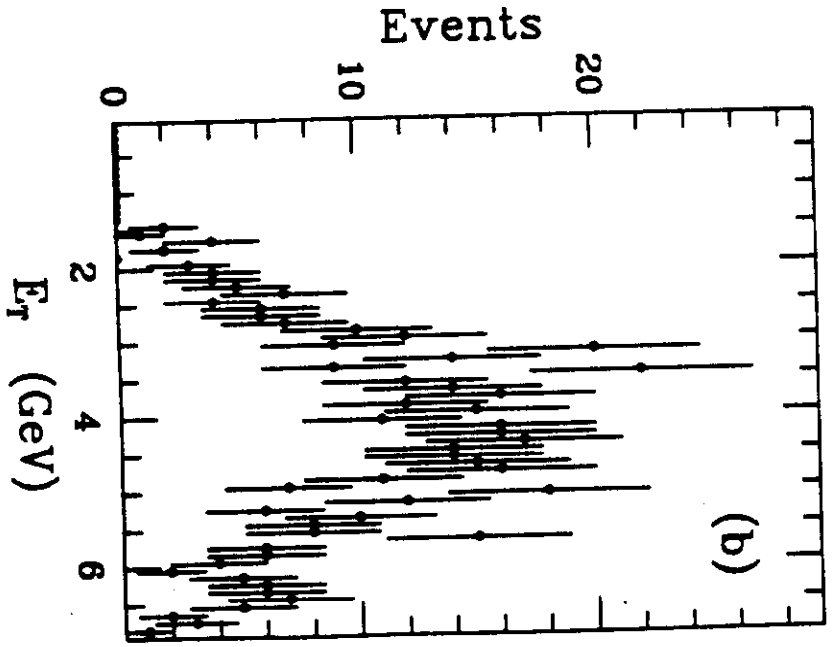

Figure 3b

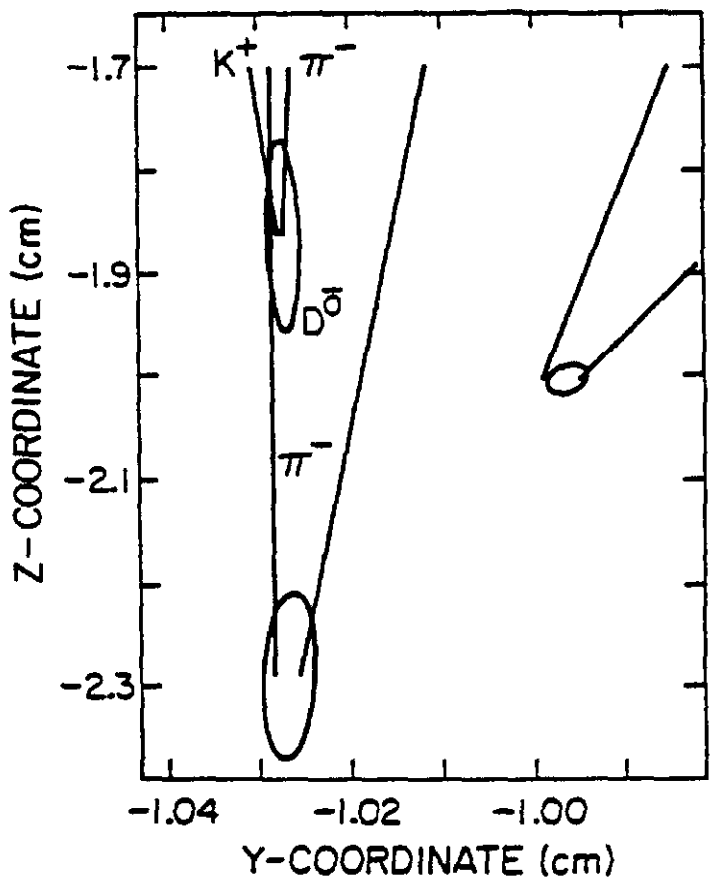

Figure 4.

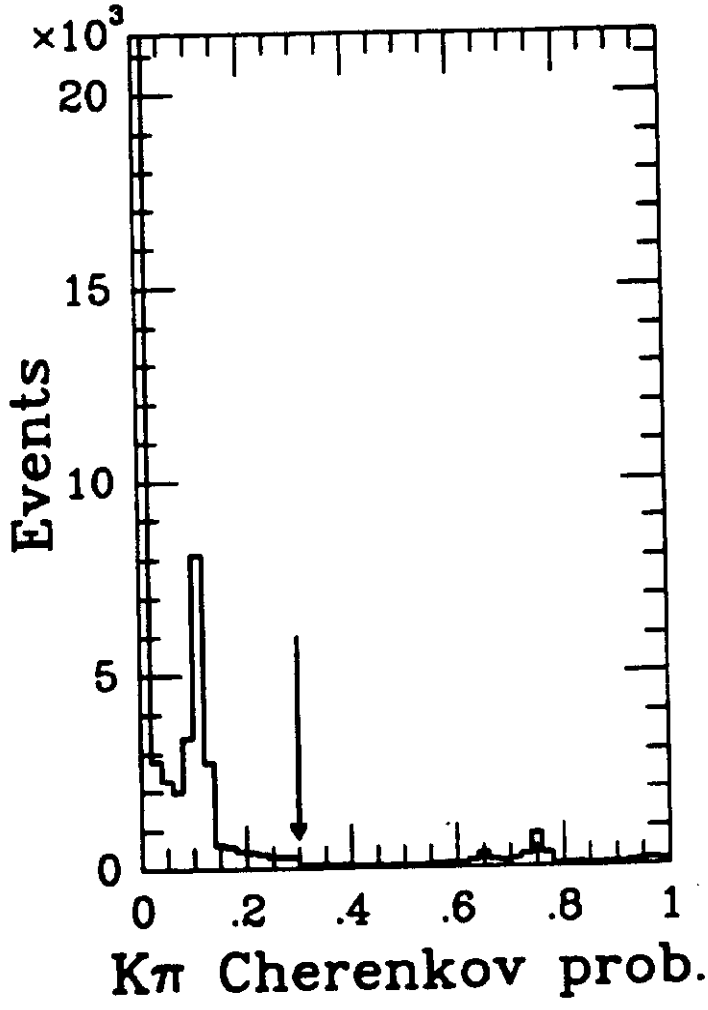

Figure 5.

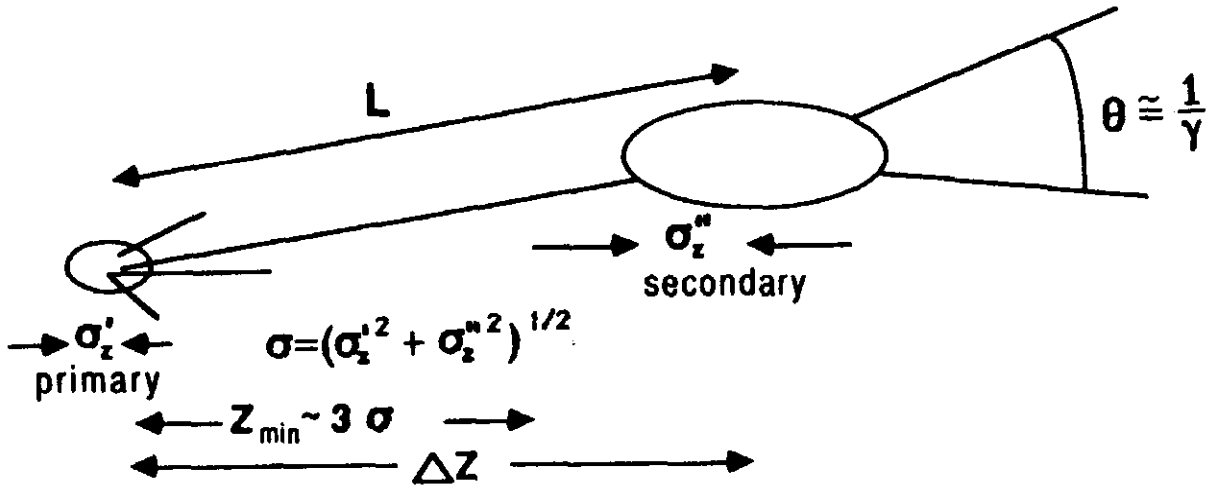

Figure 6.

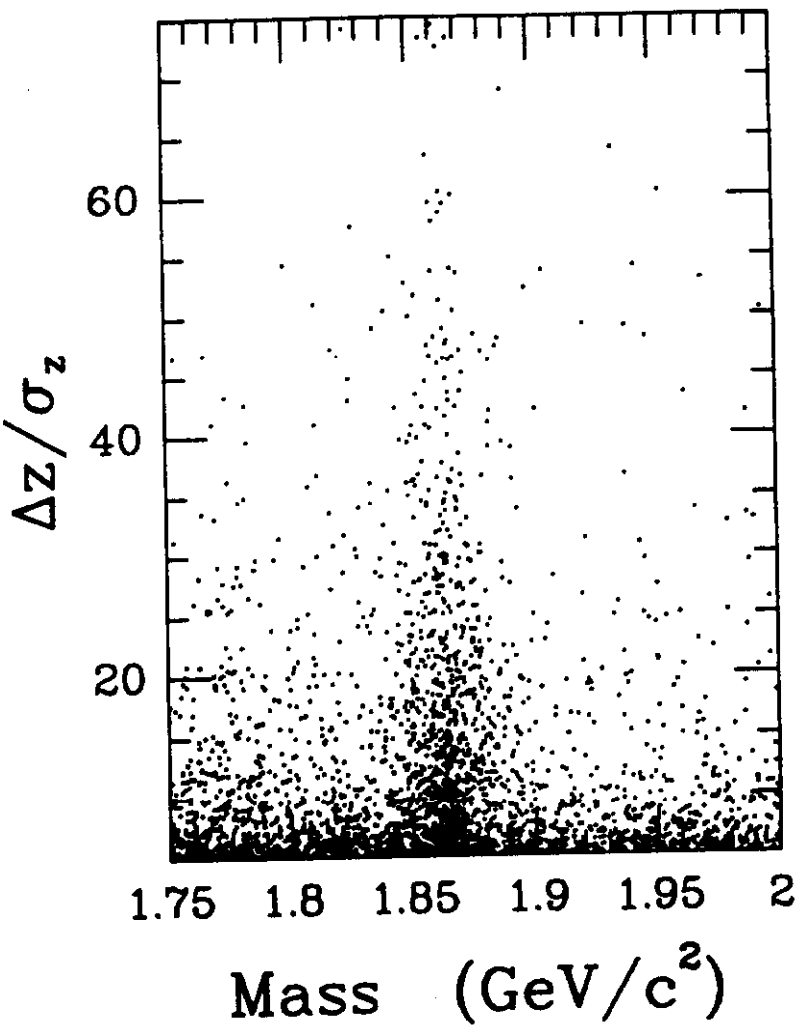

Figure 7.

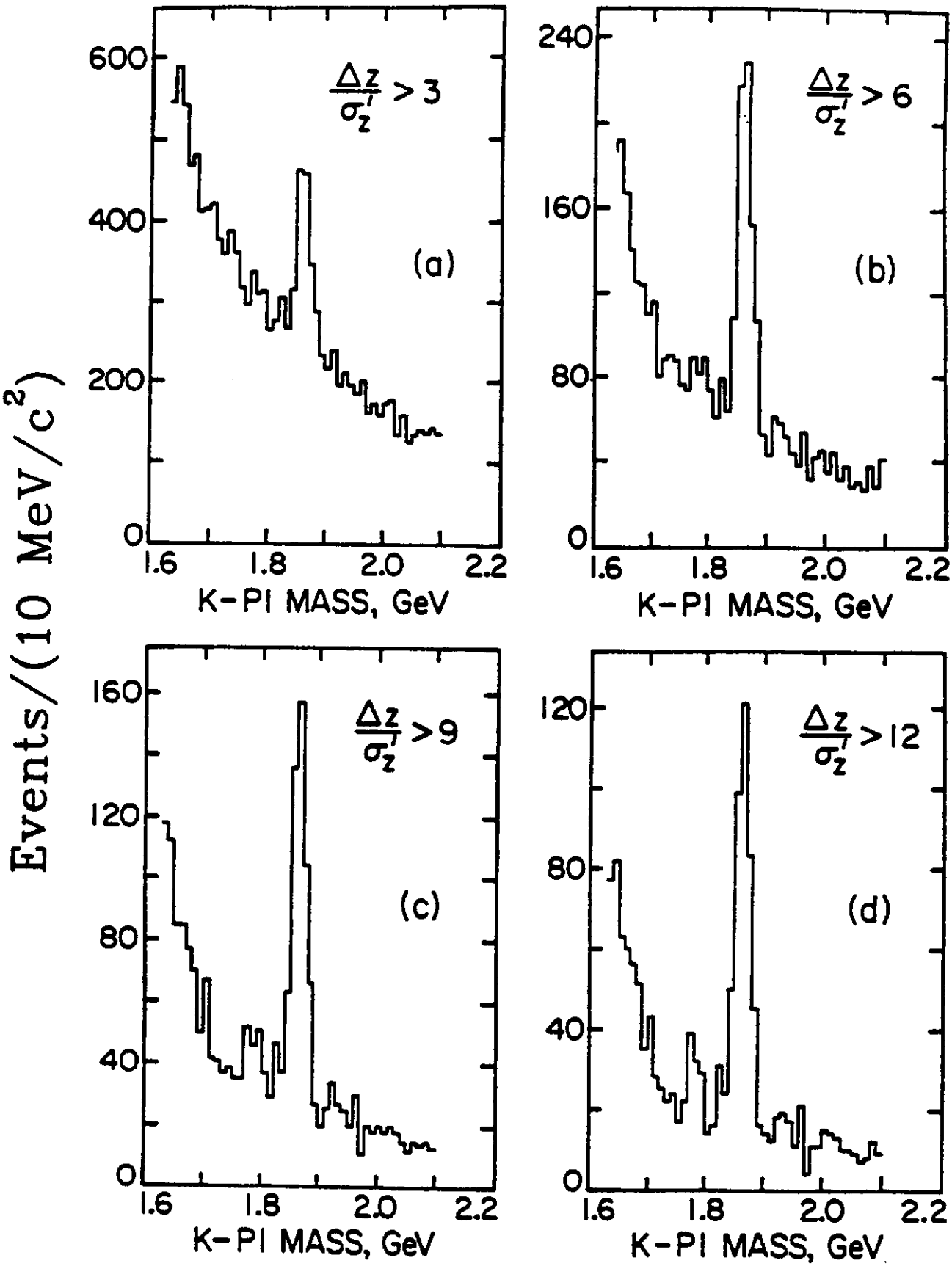
Events/(10 MeV/c²)
600
400
200
0
Δz/σz' > 3
(a)
1.6
1.8
2.0
2.2
K-PI MASS, GeV
240
160
80
0
Δz/σz' > 6
(b)
1.6
1.8
2.0
2.2
K-PI MASS, GeV
160
120
80
40
0
Δz/σz' > 9
(c)
1.6
1.8
2.0
2.2
K-PI MASS, GeV
120
80
40
0
Δz/σz' > 12
(d)
1.6
1.8
2.0
2.2
K-PI MASS, GeV

Figure 8.

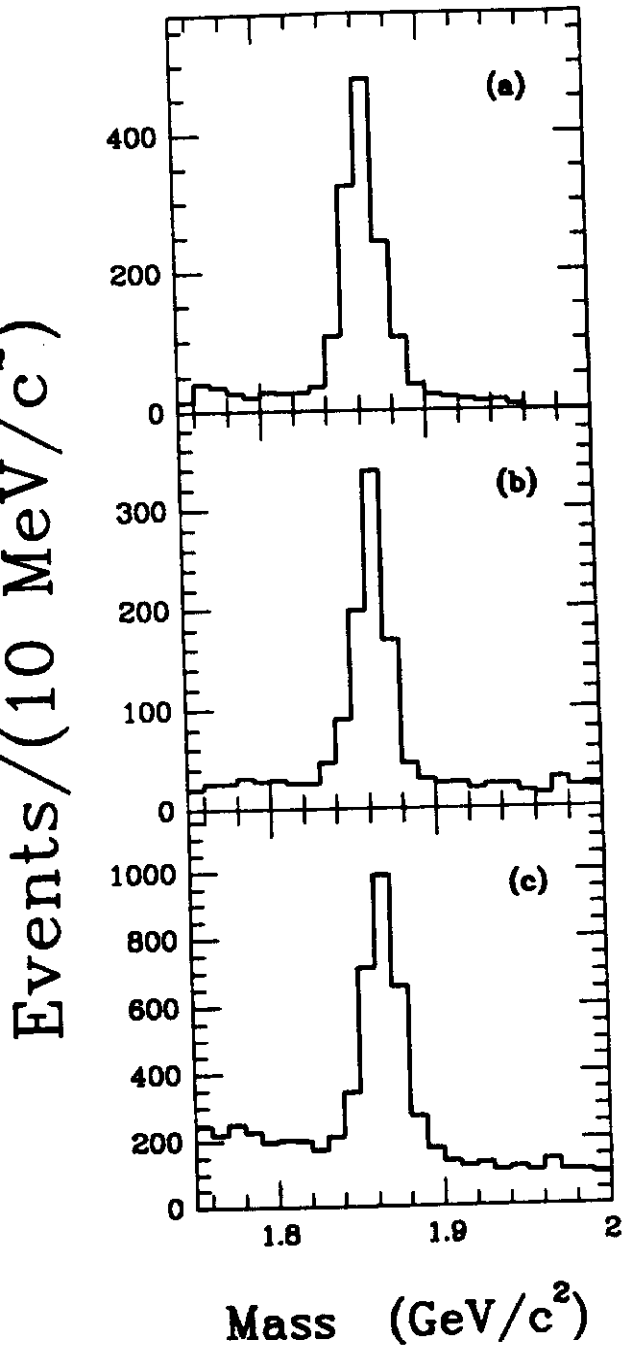
(a)
(b)
(c)
400
200
0
300
200
100
0
1000
800
600
400
200
0
1.8
1.9
2
Events/(10 MeV/c^2)
Mass (GeV/c^2)

Figure 9.

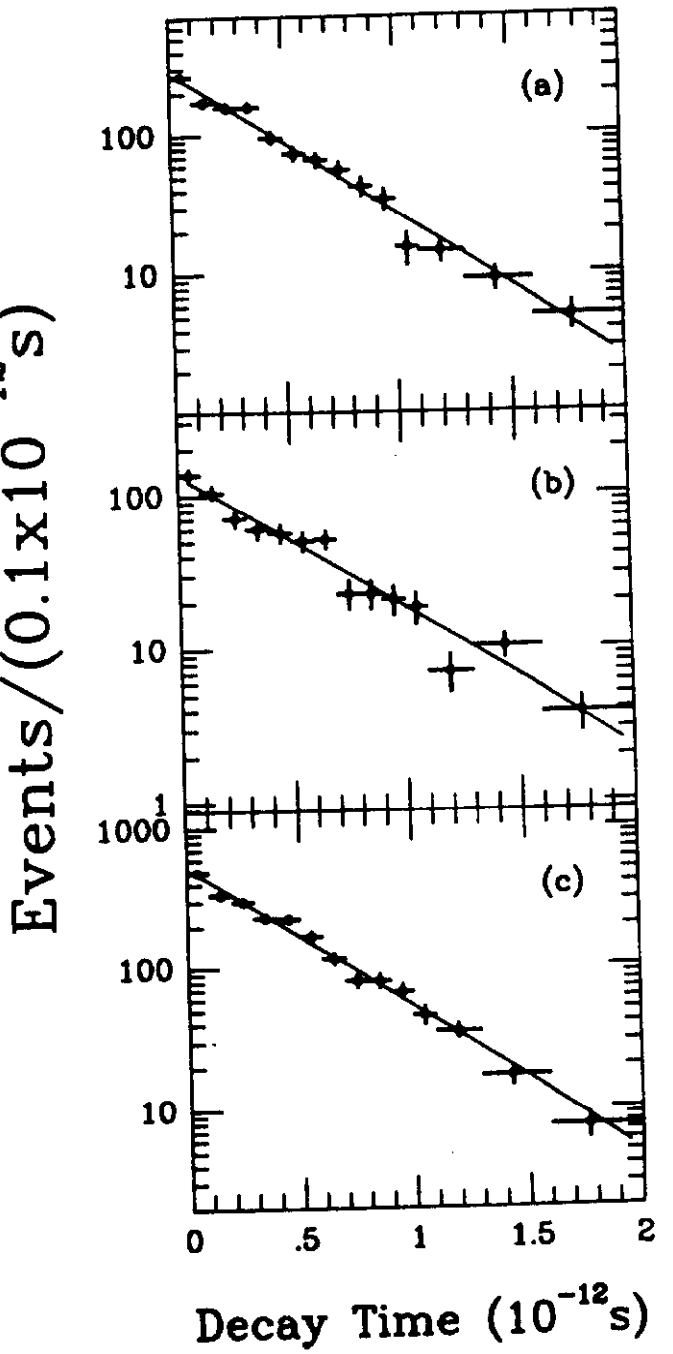

Figure 10.

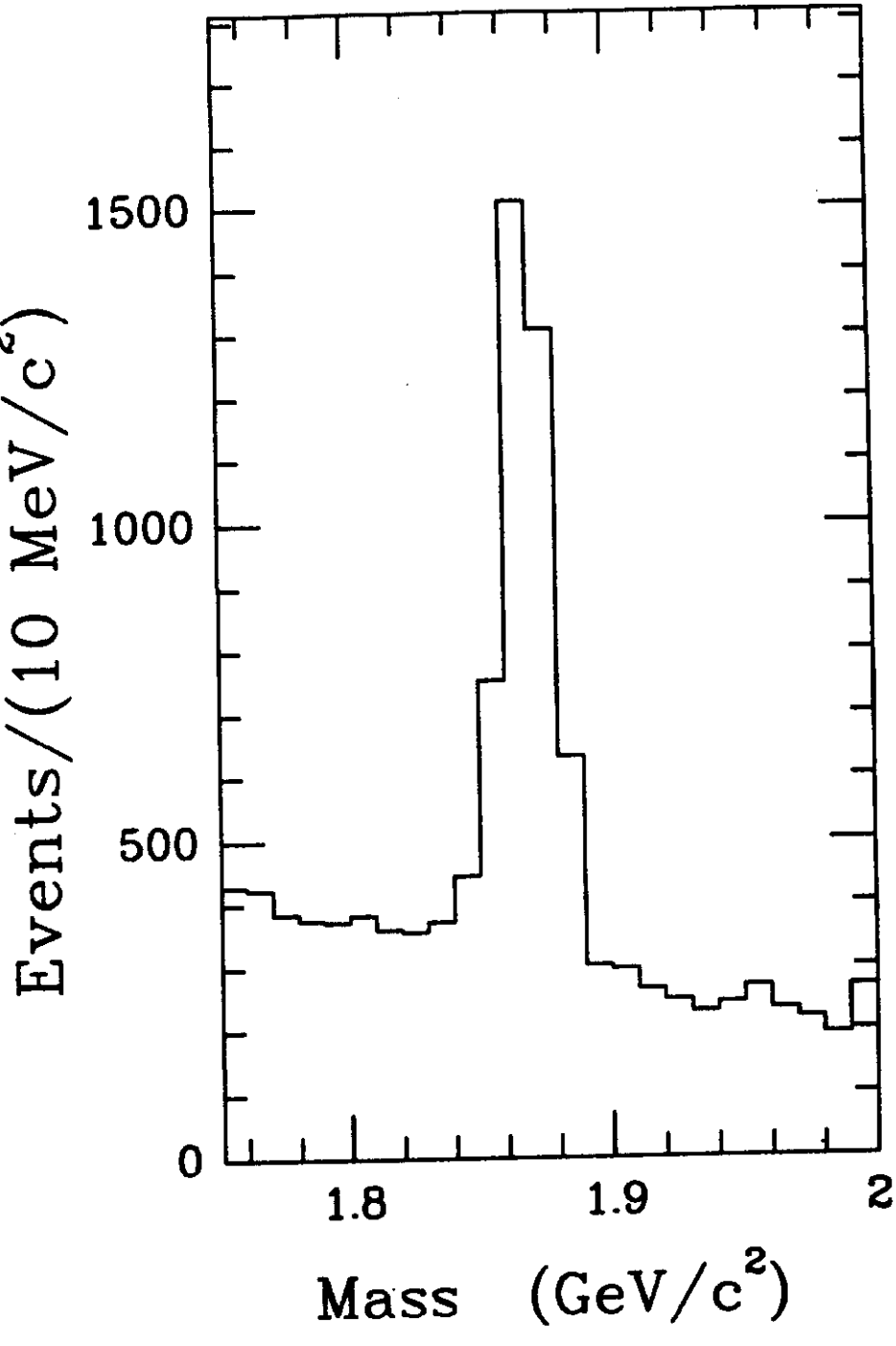

Figure 11.

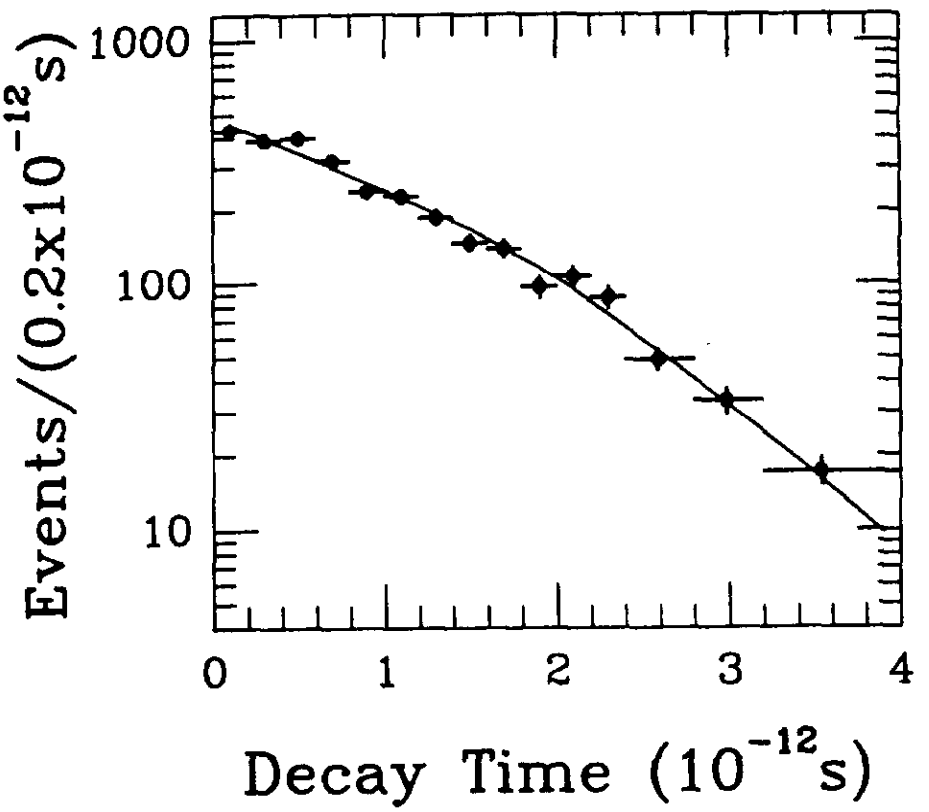

Figure 12.

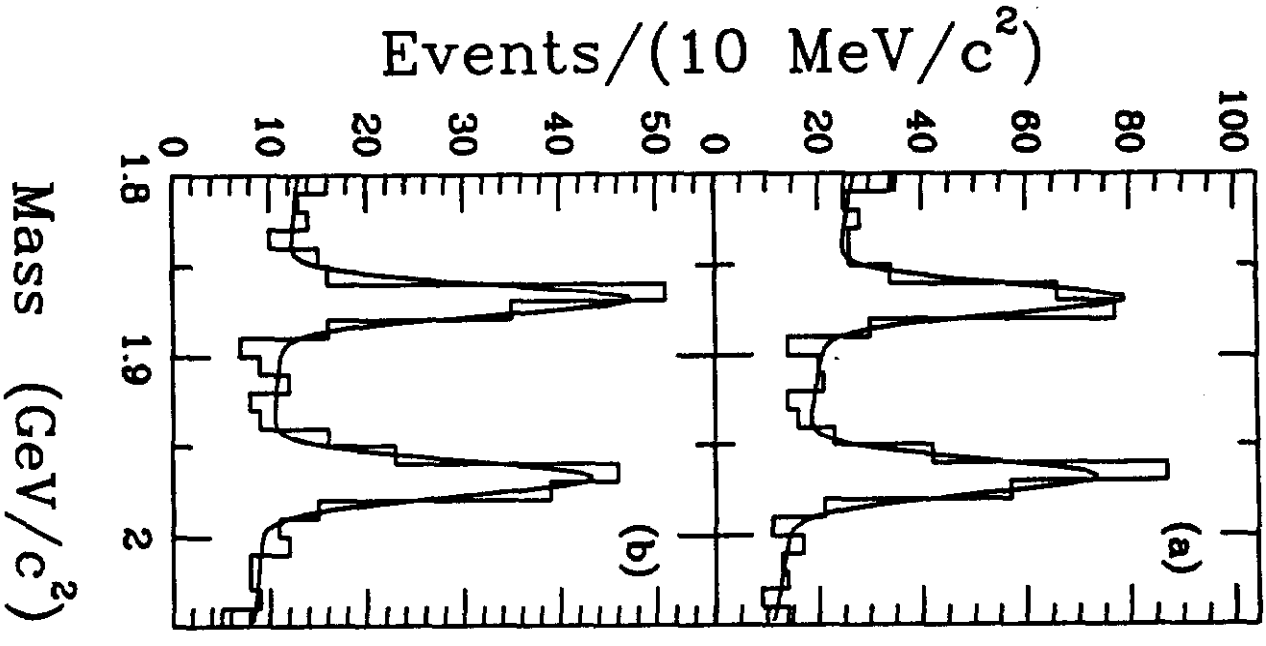
Events/(10 MeV/c²)
0
10
20
30
40
50
0
20
40
60
80
100
1.8
1.9
2
Mass (GeV/c²)
(b)
(a)

Figure 13.

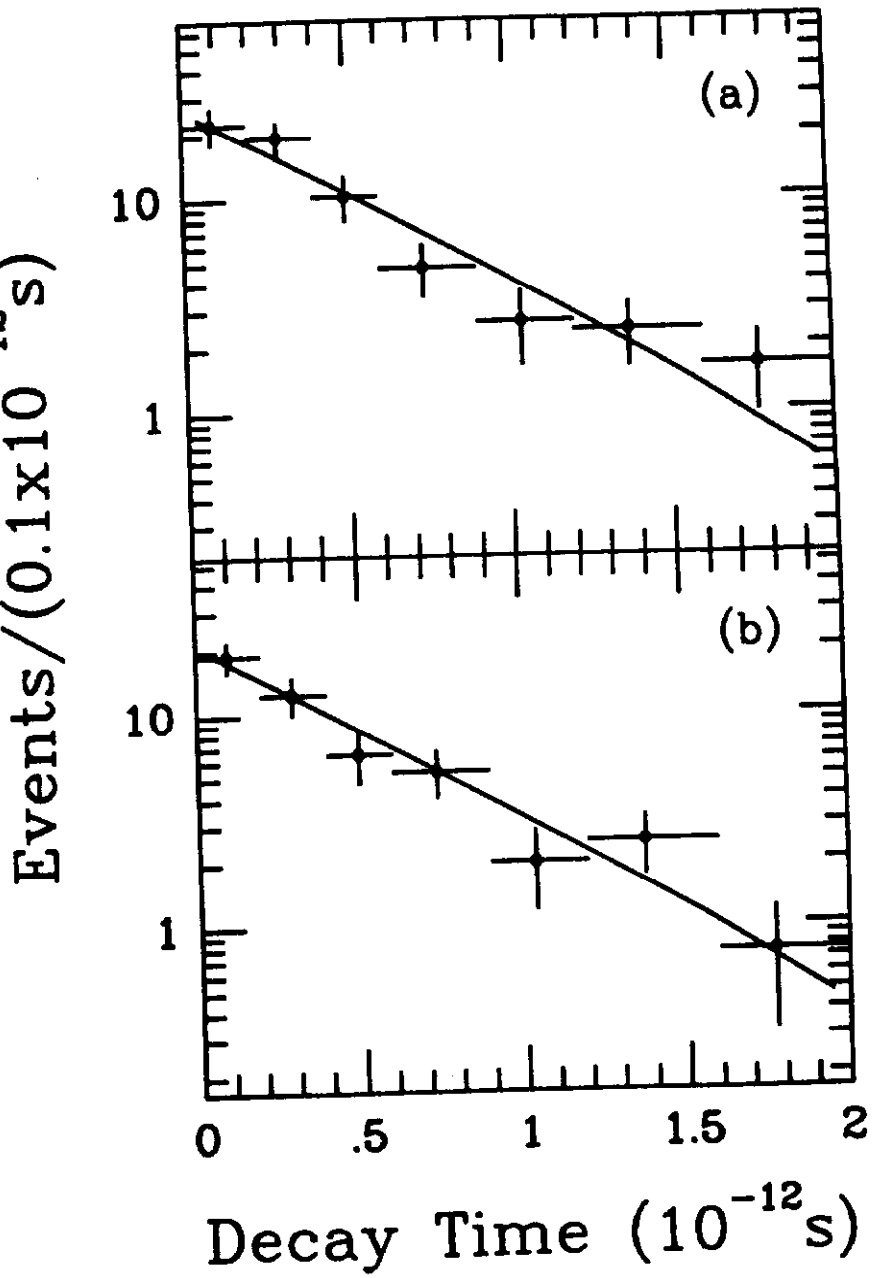

Figure 14.

Figure 15.

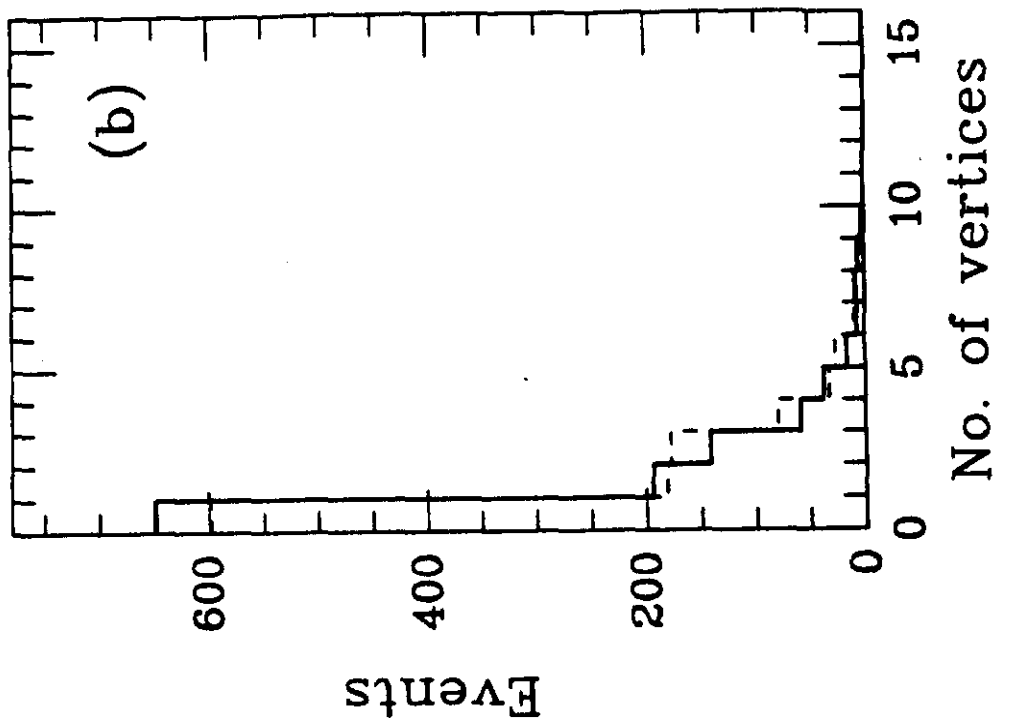
(b)
Events
600
400
200
0
0
5
10
15
No. of vertices

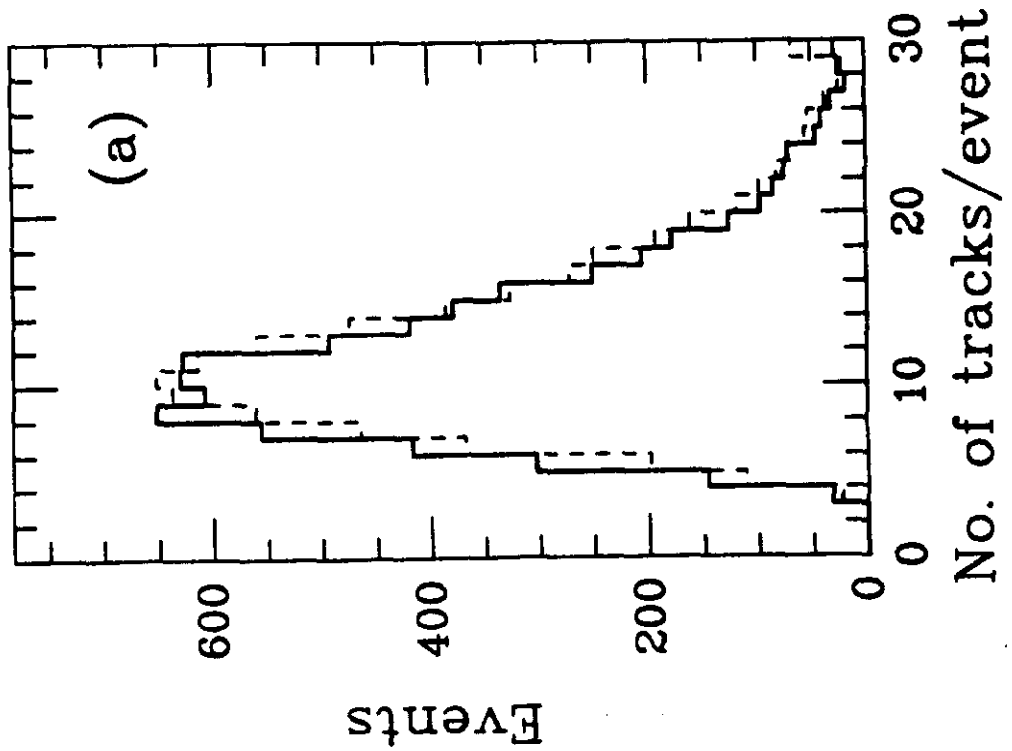
(a)
Events
600
400
200
0
0
10
20
30
No. of tracks/event

Figure 15 (cont.)

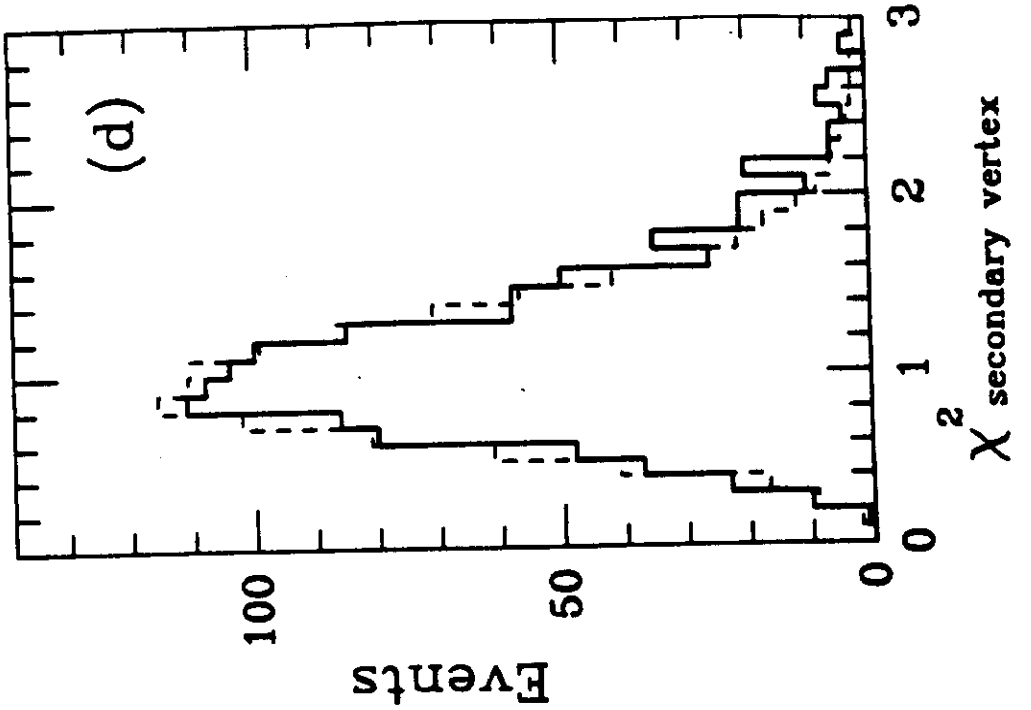

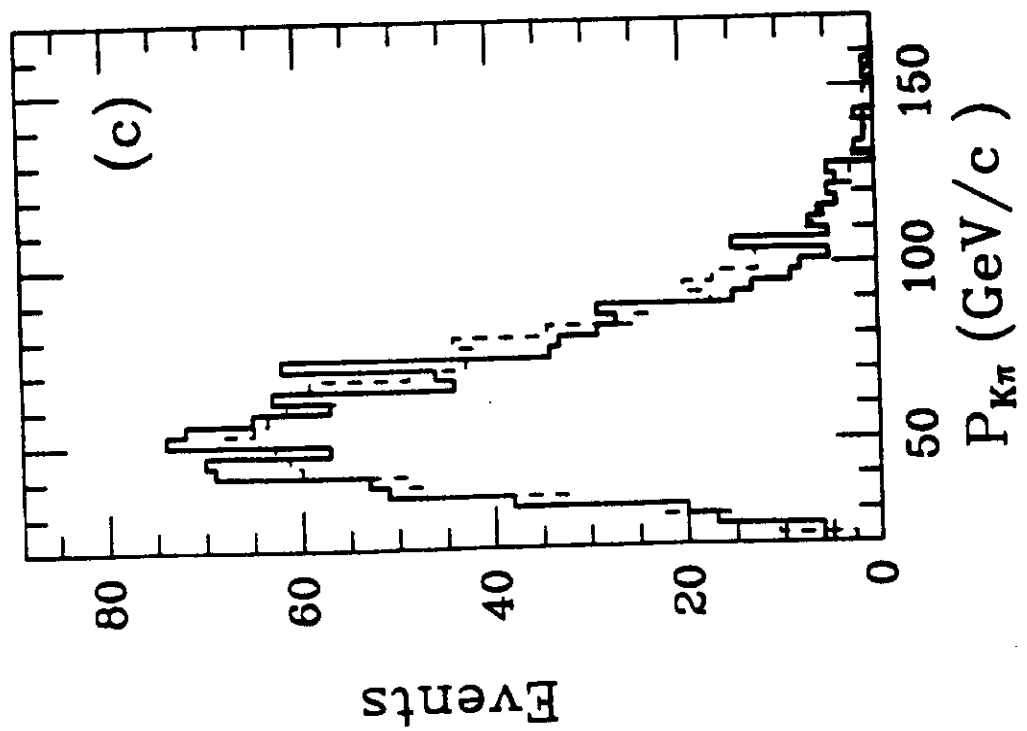

Figure 15 (cont.)

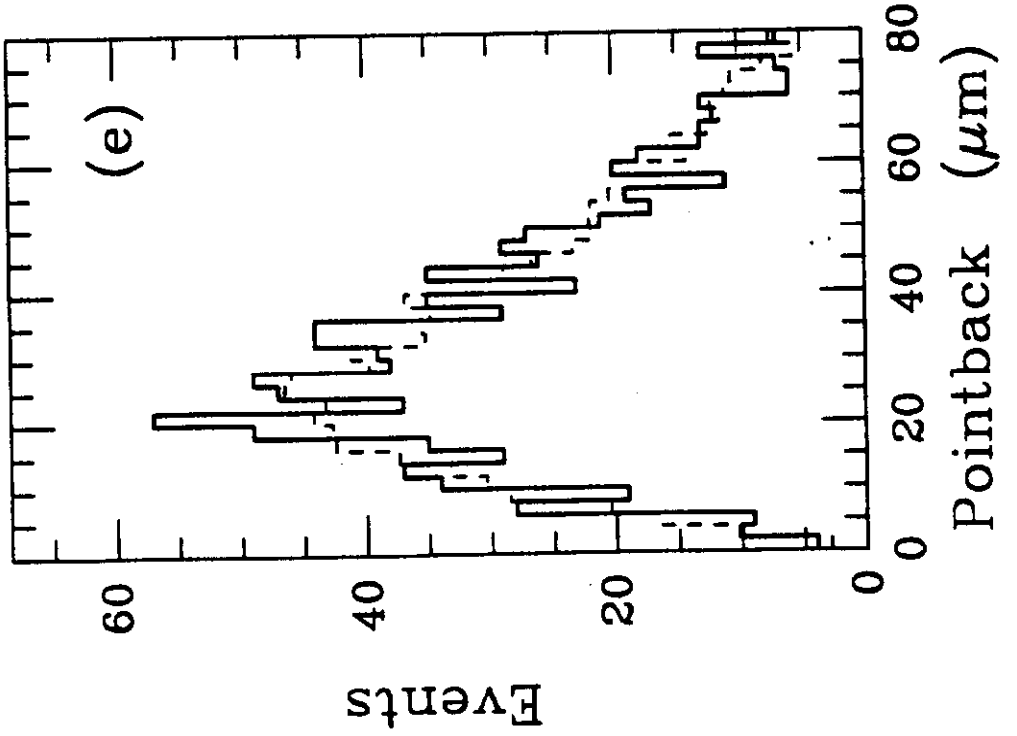

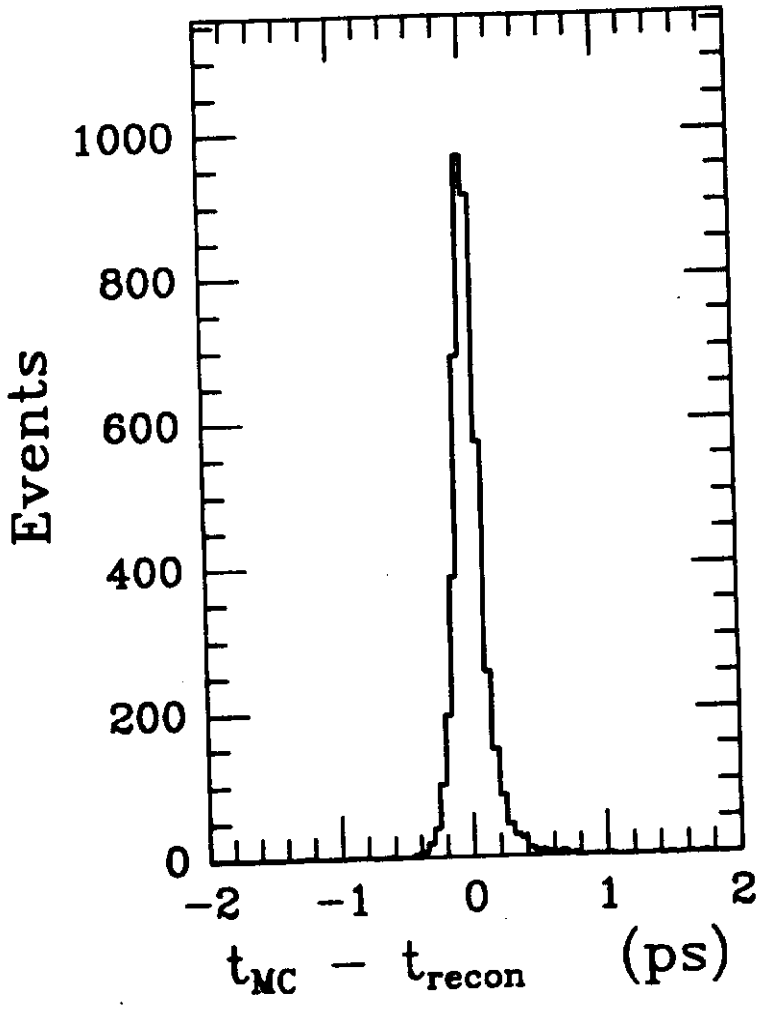

Figure 16.